arXiv:cond-mat/0310078v1 [cond-mat.mtrl-sci] 3 Oct 2003

Thermal degradation and viscoelasticity of polypropylene–clay nanocomposites

A.D. Drozdov*, A. Al-Mulla, D.A. Drozdov and R.K. Gupta
Department of Chemical Engineering
West Virginia University
P.O. Box 6102
Morgantown, WV 26506, USA

Abstract

Results of torsional oscillation tests are reported that were performed at the temperature $T = 230$ °C on melts of a hybrid nanocomposite consisting of isotactic polypropylene reinforced with 5 wt.% of montmorillonite clay. Prior to mechanical testing, specimens were annealed at temperatures ranging from $T_a = 250$ to 310 °C for various amounts of time (from 15 to 420 min). Thermal treatment induced degradation of the matrix and a pronounced decrease in its molecular weight. An integro-differential equation is derived for the evolution of molecular weight based on the fragmentation–aggregation concept. This relation involves two adjustable parameters that are found by fitting observations. With reference to the theory of transient networks, constitutive equations are developed for the viscoelastic response of nanocomposite melts. The stress–strain relations are characterized by three material constants (the shear modulus, the average energy for rearrangement of strands and the standard deviation of activation energies) that are determined by matching the dependencies of storage and loss moduli on frequency of oscillations. Good agreement is demonstrated between the experimental data and the results of numerical simulation. It is revealed that the average energy for separation of strands from temporary junctions is independent of molecular weight, whereas the elastic modulus and the standard deviation of activation energies linearly increase with mass-average molecular weight.

Key-words: Isotactic polypropylene, Montmorillonite clay, Nanocomposites, Thermal degradation, Viscoelasticity

*E–mail: Aleksey.Drozdov@mail.wvu.edu

Introduction

This paper is concerned with (i) the kinetics of thermal degradation of a hybrid nanocomposite with isotactic polypropylene (iPP) matrix reinforced with montmorillonite (MMT) clay and (ii) the effect of degradation on the viscoelastic response of the nanocomposite in the melt state.

The choice of iPP for the experimental analysis is explained by numerous industrial applications of this semicrystalline polymer (oriented films for packaging, reinforcing fibres, non-woven fabrics, pipes, etc.). Montmorillonite is an inorganic clay conventionally used for preparation of hybrid nanocomposites. It possesses a layered structure constructed of two tetrahedral sheets of silica surrounding an octahedral sheet of alumina or magnesia. The layers (with a thickness of 1 nm) are stacked by weak dipole forces, while the galleries between the layers are occupied by metal cations.

The focus on the influence of thermal degradation of a polymer–clay nanocomposite on its time-dependent response may be explained by two reasons: (i) from the standpoint of applications, the effect of degradation on the viscoelastic behavior is of essential importance for the prediction of mechanical properties of reprocessed industrial and post-consumer plastic wastes [1]; (ii) from the point of view of fundamental research, thermal degradation of a polymer is tantamount to a reduction in its molecular weight [2], which implies that the analysis of the time-dependent response of nanocomposite melts annealed at various temperatures $T_{\rm a}$ for various amounts of time $t_{\rm a}$ sheds some light on their structure–property relations (correlations between the molecular weight of the matrix and the material parameters describing the mechanical response).

The kinetics of thermal and thermo-oxidative degradation of polypropylene has attracted substantial attention in the past decade, see [3, 4, 5, 6], to mention a few. Annealing, thermal degradation and stability of nanocomposites with a polypropylene matrix and MMT filler were recently studied in [7, 8, 9, 10, 11, 12, 13]. Some relations between the viscoelastic response of iPP–MMT nanocomposites and their structure have been established in [14, 15, 16, 17].

Despite substantial progress in our understanding of the degradation process and its effect on the mechanical response of hybrid nanocomposites, it is difficult, however, to mention a constitutive model that adequately predicts the time-dependent behavior of iPP–MMT nanocomposite annealed for a given time $t_{\rm a}$ at a required temperature $T_{\rm a}$ above the melting temperature $T_{\rm m}$.

The objective of this study is three-fold:

1. To report experimental data in isothermal torsional oscillation tests with small strains (at the temperature $T = 230$ °C, which is a typical temperature for injection-molding of iPP) on specimens annealed for various amounts of time $t_{\rm a}$ (ranging from 15 to 420 min) at various temperatures $T_{\rm a}$ (in the interval from 250 to 310 °C).

2. To develop kinetic equations for the evolution of number-average and mass-average molecular weights at thermal degradation and to find adjustable parameters in these relations by fitting the experimental data.

3. To derive constitutive equations for the viscoelastic behavior of a nanocomposite melt, to determine material constants in the stress–strain relations by matching the dependencies of the storage and loss moduli on frequency, and to evaluate the effect of thermal degradation on the time-dependent response.

To make the model tractable from the mathematical standpoint, we adopt the homogenization hypothesis. According to it, a complicated micro-structure of a nanocomposite may be replaced by an equivalent phase, whose response captures essential features of the mechanical behavior of the nanocomposite. As the equivalent phase, a network of macromolecules is chosen in the present study.

Following [18, 19, 20], degradation of the host matrix in an hybrid nanocomposite is treated as a combination of two thermally-activated processes: (i) binary scission of chains, and (ii) annihilation of end- and side-groups (diffusion of small-size fragmentation products and their subsequent evaporation through the surface of a specimen). To simplify the analysis, we accept the conventional assumptions that (i) the probability of a scission event is independent of a chain's length and the position of a bond along the backbone of a chain; (ii) the diffusivity of separated end- and side-groups is so large at the exposure temperature $T_{\rm a}$ that the kinetics of diffusion of oligomers and their evaporation may be disregarded. As a result, the number of material constants in the kinetic equation is reduced to two. These quantities are found by matching a master-curve for the decrease in the mass-average molecular weight with exposure time $t_{\rm a}$.

To develop constitutive equations for a nanocomposite melt, we accept the concept of transient networks [21, 22, 23, 24]. The melt is treated as a network of strands bridged by temporary junctions (entanglements and physical cross-links on the surfaces of clay platelets). At random times, active strands separate from their junctions being excited by thermal fluctuations, and dangling strands merge with the network. Following [25, 26], we assume the network to be strongly heterogeneous in the sense that different junctions are characterized by different activation energies for detachment of strands. The theory of temporary networks has been applied to describe the time-dependent behavior of polypropylene in the solid state in [25, 27, 28, 26], to mention a few. The previous studies, however, did not pay much attention to the effect of molecular weight on material parameters in the constitutive equations. The fact that the viscoelastic response of polypropylene melts is strongly affected by the distribution of chains' lengths has been established experimentally in [29, 30, 31, 32, 33, 34]. The aim of this work is to evaluate the influence of mass-average molecular weight on (i) the concentration of active strands in an equivalent network, and (ii) the distribution function for temporary junctions with various activation energies.

The exposition is organized as follows. First, experimental data in torsional oscillation tests are reported on annealed specimens, and their mass-average molecular weight is determined by using observations for complex viscosity. Afterwards, kinetic equations are developed for changes in the concentration of chains with various lengths induced by thermal treatment. Adjustable parameters in these equations are determined by fitting the observations for molecular weight. We proceed with the derivation of stress–strain relations for an heterogeneous transient network at three-dimensional deformations with small strains. The constitutive equations involve three material constants that are found by matching the data for storage and loss moduli as functions of frequency of oscillations. Finally, we establish correlations between the adjustable parameters in the stress–strain relations and the mass-average molecular weight of the polypropylene matrix and discuss the physical meaning of these relationships.

Experimental procedure

Isotactic polypropylene PP 1012 (density 0.906 g/cm^3, melt flow rate 1.2 g/10 min) was purchased from BP Amoco Polymers, Inc. Concentrate C–44PA containing 43 wt.% of intercalated montmorillonite clay in de-agglomerated form was supplied by Nanocor Co.

To prepare hybrid nanocomposite with 5 wt.% of MMT clay, appropriate amounts of isotactic polypropylene and the concentrate were dried overnight at the temperature $T = 100$ °C, pellets were mixed and melt-blended in a twin-screw extruder (Brabender Instruments, Inc.) with a screw rate of 30 rpm and temperatures in the extruder barrel of 260, 290, 300 and 290 °C from hopper to die, respectively. Strands from the extruder were cooled in a water bath, cut with a pelletizer, and dried in an oven at 100 °C for 12 h. Circular plates with diameter 64 mm and thickness 3 mm were molded in injection-molding machine Battenfeld 1000/315 CDC (Battenfeld). Specimens for mechanical tests (with diameter 30 mm) were cut from the plates.

Our choice of the concentration of MMT clay in the hybrid nanocomposite ($\phi = 5$ wt.%) is explained by the fact that this amount of nanoclay is sufficient to improve substantially mechanical properties of neat polypropylene. According to [16], the tensile strength of iPP–MMT nanocomposite reaches its maximum when the clay concentration equals 5 wt.%. Another reason for this choice is that reinforcement of conventional polymers with MMT clay at higher concentrations of filler practically does not improve their thermal stability [35].

To evaluate the melting temperature T_m of the matrix and the nanocomposite, DSC (differential scanning calorimetry) measurements were preformed by using DSC 910S apparatus (TA Instruments). The calorimeter was calibrated with indium as a standard. Two specimens of neat iPP and iPP–MMT nanocomposite with weights of approximately 13 mg were tested with a heating rate of 10 K/min from room temperature to 200 °C under nitrogen. The melting temperature $T_\mathrm{m} = 172$ °C was determined for isotactic polypropylene as the point corresponding to the peak on the melting curves. No substantial changes in the melting temperature were found for the nanocomposite. This conclusion is in agreement with the results of previous studies [13].

To analyze lattice spacing in the montmorillonite clay and changes in the crystalline morphology of iPP driven by the presence of filler, X–ray diffraction tests were performed on isotactic polypropylene and polypropylene–clay nanocomposite by using Rugaku D-max B diffractometer with Cu–K_α radiation ($\lambda = 1.54$ Å) generated by a tube with a voltage of 40 kV and a current of 30 mA. The Bragg scattering angle ranged from $2\Theta = 3$ to $2\Theta = 60°$ with the step of 0.06°. The diffraction spectrum of the hybrid nanocomposite revealed two peaks: a rather large and wide intensity maximum at $2\Theta = 3.0°$ (the basal spacing of 30 Å) and a smaller one at $2\Theta = 6.5°$ (the basal spacing of 17 Å). The presence of these peaks indicated a high level of intercalation of polymer chains between clay platelets. These observations are similar to those found by other researchers [14, 16, 17, 36] on iPP–MMT nanocomposites with similar concentrations of clay.

Among other interesting features of the X-ray diffractograms, we would mention: (i) an increase in $\alpha(110)$ peak of the nanocomposite compared to that of iPP (by a factor of 5), (ii) the growth of $\alpha(040)$ peak (by a factor of 3.3), (iii) a decrease in $\alpha(130)$ peak (by 26 %), (iv) the formation of $\gamma(117)$ peak at $2\Theta = 19.6°$, (v) the disappearance of $\alpha(111)$ and $\alpha(-131)$ peaks, and (vi) a strong growth of $\alpha(060)$ peak at $2\Theta = 25.2°$ (by a factor of 3.5).

It is worth noting that a pronounced reduction in the diffraction peaks at $2\Theta = 21.2°$

was recently reported in [37] for hot-stretched polypropylene samples. It was associated with preferential orientation of crystallites driven by deformation of specimens. With reference to this assertion, the fact that the $\alpha(111)$ and $\alpha(-131)$ peaks were not observed in the nanocomposite may be ascribed to the effect of anisotropically distributed clay platelets on the orientation of lamellar blocks in injection-molded samples.

Dynamic tests were performed by using RMS-800 rheometric mechanical spectrometer with parallel disks (diameter 25 mm, gap length 2 mm). The shear storage modulus G' and the shear loss modulus G'' were measured in oscillation tests (the frequency-sweep mode) with the amplitude of 15 % and various frequencies ω ranging from 0.1 to 100 rad/s. The choice of the amplitude of oscillations was driven by the following requirements: (i) mechanical tests were performed in the region of linear viscoelasticity, and (ii) the torque was less than its ultimate value 0.2 N·m. The limitation on the minimum frequency of oscillations was imposed by the condition that the torque exceeded its minimum value $2.0 \cdot 10^{-4}$ N·m. To check that the storage and loss moduli were not affected by the strain amplitude, several tests were repeated with the amplitude of 5 %. No change in the dynamic moduli was observed. The temperature in the chamber was controlled with a standard thermocouple that showed that the temperature of specimens remained practically constant (with the accuracy of ± 0.5 °C).

Prior to mechanical tests, specimens were annealed in the spectrometer at the temperatures $T_a = 250$, 270, 290 and 310 °C (with gap length 3 mm) for various amounts of time t_a ranging from 15 min to 7 h (420 min). After thermal treatment of a specimen, the temperature was reduced to the test temperature $T = 230$ °C, the specimen was thermally equilibrated (during 5 min), the gap length was reduced to 2 mm, an extraneous material was carefully removed, and the shear storage and loss moduli were measured at various frequencies ω starting from the lowest one. Each test was performed on a new specimen.

We suppose that squeezing of samples between plates of the spectrometer and removal of the extraneous material substantially reduced the effect of thermo-oxidative degradation (compared to that of thermal degradation) on the mechanical response, because the major part of the material where oxidative degradation occurred was taken away (about one third of the initial mass of each specimen). However, we cannot exclude entirely the effect of diffusion of oxygen to the central part of the samples, in particular, at the highest temperatures ($T_a = 290$ and 310 °C) used in the experiments [38].

The storage G' and loss G'' moduli, as well as the modulus of the complex viscosity η are plotted versus the logarithm ($\log = \log_{10}$) of frequency ω in Figures 1 to 12 (conventional semi-logarithmic plots are used to characterize changes in these quantities with frequency). The shapes of the curves presented coincide qualitatively with those reported by other researchers, see, e.g., [15]. Given an annealing time t_a and an annealing temperature T_a, the storage modulus G' and the loss modulus G'' strongly increase with frequency, whereas the complex viscosity η noticeably decreases with ω. For a fixed frequency ω, the dynamic moduli are pronouncedly reduced with t_a and T_a.

Evaluation of molecular weight

To assess changes in the molecular weight of the hybrid nanocomposite induced by thermal degradation of the matrix, the experimental dependencies $\eta(\omega)$ depicted in Figures 3, 6, 9 and

12 are approximated by the Cross model

$$\eta(\omega) = \eta_\infty + \frac{\Delta\eta}{1 + (\tau\omega)^\alpha}, \tag{1}$$

where η_∞ is the high-frequency complex viscosity ($\omega \to \infty$), $\Delta\eta = \eta_0 - \eta_\infty$, η_0 is the zero-frequency complex viscosity ($\omega = 0$), and α and τ are adjustable parameters.

Each curve $\eta(\omega)$ is approximated separately. To find the constants η_∞, $\Delta\eta$, α and τ in Eq. (1), we fix some intervals $[0, \alpha_{\max}]$ and $[0, \tau_{\max}]$, where the "best-fit" parameters α and τ are assumed to be located, and divide these intervals into J subintervals by the points $\alpha^{(i)} = i\Delta\alpha$ and $\tau^{(j)} = j\Delta\tau$ ($i, j = 1, \ldots, J-1$) with $\Delta\alpha = \alpha_{\max}/J$ and $\Delta\tau = \tau_{\max}/J$. For any pair $\{\alpha^{(i)}, \tau^{(j)}\}$, the coefficients η_∞ and $\Delta\eta$ in Eq. (1) are found by the least-squares method from the condition of minimum of the function

$$F = \sum_{\omega_m} \Big[\eta_{\exp}(\omega_m) - \eta_{\text{num}}(\omega_m)\Big]^2,$$

where the sum is calculated over all experimental points ω_m depicted in Figures 3, 6, 9 and 12, $\eta_{\exp}$ is the complex viscosity measured in a test, and η_{num} is given by Eq. (1). The "best-fit" parameters α and τ are determined from the condition of minimum of the function F on the set $\{\alpha^{(i)}, \tau^{(j)} \quad (i, j = 1, \ldots, J-1)\}$. After finding the "best-fit" values $\alpha^{(i)}$ and $\tau^{(j)}$, this procedure is repeated twice for the new intervals $[\alpha^{(i-1)}, \alpha^{(i+1)}]$ and $[\tau^{(j-1)}, \tau^{(j+1)}]$, to ensure an acceptable accuracy of fitting. Figures 3, 6, 9 and 12 demonstrate good agreement between the experimental data and the results of numerical simulation.

After finding the zero-frequency viscosity η_0, the mass-average molecular weight M_{w} is determined by the conventional equation [39]

$$\frac{\eta_0}{\eta_0^{\text{ref}}} = \left(\frac{M_{\text{w}}}{M_{\text{w}}^{\text{ref}}}\right)^{3.4}, \tag{2}$$

where η_0^{ref} and $M_{\text{w}}^{\text{ref}}$ are the zero-frequency viscosity and the mass-average molecular weight of a reference (not subjected to thermal treatment) specimen. The ratio of mass-average molecular weights

$$d_{\text{w}} = \frac{M_{\text{w}}}{M_{\text{w}}^{\text{ref}}}$$

is found from Eq. (2) by using the experimental data for η_0. This method of determining the ratio of mass-average molecular weights of polypropylene was previously used in [40].

It is worth noting that Eq. (2) is traditionally employed for the evaluation of molecular weight of neat polymers. Its applicability to melts of hybrid nanocomposites is grounded on the conventional models in rheology of particulate suspensions [41], which presume that the relative viscosity (the ratio of the viscosity of a suspension to that of the neat polymer melt) is independent of the melt's structure and is determined by the concentration of filler exclusively.

The ratio d_{w} is plotted versus annealing time t_{a} in Figure 13. With reference to [3, 20], we accept the time–temperature superposition principle for degradation of the nanocomposite. According to this hypothesis, the dependencies $d_{\text{w}}(t_{\text{a}})$ measured at various annealing temperatures T_{a} and plotted in semi-logarithmic coordinates (d_{w} versus $\log t_{\text{a}}$) may be superposed

with an acceptable level of accuracy by shifting the observations along the time-axis. Applying this approach, we construct the master-curve depicted in Figure 13. The experimental data at $T_{\rm a}^{\rm ref} = 290$ °C are presented without changes. Observations at the other temperatures ($T_{\rm a} = 250$, 270 and 310 °C) are shifted along the time-axis by appropriate amounts A that are determined from the condition that the experimental data produce a smooth master-curve.

The parameter A is plotted versus the absolute temperature $T_{\rm a}$ in Figure 14. The experimental data are approximated by the Arrhenius dependence

$$\ln A = A_0 - \frac{A_1}{T_{\rm a}}, \tag{3}$$

where the coefficients A_i $(i = 0, 1)$ are determined by the least-squares method. Figure 14 demonstrates that Eq. (3) ensures quite acceptable fit of the observations.

For each annealing time $t_{\rm a}$ and annealing temperature $T_{\rm a}$, we (i) calculate the material constants α and τ in Eq. (1) by matching the observations depicted in Figures 3, 6, 9 and 12, (ii) find the ratio of mass-average molecular weights $d_{\rm w}$ from Eqs. (1) and (2), and (iii) plot the adjustable parameters α and τ versus $d_{\rm w}$ in Figures 15 and 16. The experimental data are approximated by the phenomenological relations

$$\alpha = \alpha_0 - \alpha_1 d_{\rm w}, \qquad \tau = \tau_0 + \tau_1 d_{\rm w}, \tag{4}$$

where the coefficients α_i and τ_i $(i = 0, 1)$ are found by the least-squares technique. Figures 15 and 16 reveal that Eq. (4) provides reasonable quality of matching the observations. The exponent α in Eq. (1) slightly decreases with mass-average molecular weight, whereas the characteristic time τ strongly grows with $M_{\rm w}$.

Kinetic equations

Our aim now is to develop kinetic equations for thermal degradation of a hybrid nanocomposite and to find adjustable parameters in these relations by matching the experimental data depicted in Figure 13. For this purpose, we (i) adopt a homogenization method, according to which a complicated micro-structure of a polymer–clay nanocomposite may be replaced by an equivalent network of macromolecules, and (ii) accept the fragmentation–annihilation concept. The latter means that the degradation process is treated as a combination of two thermally-induced processes: binary fragmentation of chains and annihilation (subsequent breakage, diffusion and evaporation through the surface of a sample) of end- and side-groups.

Binary scission of chains

Denote by $\bar{N}(t)$ the number of macromolecules per unit mass of an equivalent network at an arbitrary instant $t \geq 0$. Following common practice, we treat chains as sequences of segments connected by bonds. Denote by $N_k(t)$ is the number of chains (per unit mass) at time t containing k segments $(k = 1, 2, \ldots)$. The functions $N_k(t)$ obey the conservation law

$$\bar{N}(t) = \sum_{k=1}^{\infty} N_k(t). \tag{5}$$

Binary scission (fragmentation) of chains is described by the reactions

$$N_k \to N_l + N_{k-l} \qquad (l = 1, \ldots, k-1).$$

Denote by γ the rate of scission (the number of scission events per bond between segments per unit time). Assuming γ to be a function of temperature T only (which implies that γ is independent of the number of segments in a chain), we arrive at the kinetic equations for the functions $N_k(t)$

$$\frac{dN_k}{dt}(t) = -\gamma(k-1)N_k(t) + 2\gamma \sum_{j=k+1}^{\infty} N_j(t). \tag{6}$$

The coefficient $k-1$ in the first term describes the number of possible scission events in a chain containing k segments. The coefficient "2" before the sum in Eq. (6) indicates that there are two opportunities ("left" and "right") to obtain a chain with k segments after scission of a chain with a larger number of segments.

Annihilation of chains

Thermal fluctuations in a network induce not only binary scission of macromolecules, but also detachment of end- and side-groups from polymer chains. As these groups are rather small, they have relatively large diffusivity, and can easily leave a polymer specimen. A decrease in a sample's mass with time driven by separation and subsequent desorption of end- and side-groups and is treated as their annihilation.

Following [18, 19], we suppose that detachment of small groups within the interval $[t, t+dt]$ may be thought of as transformation of a chain with k segments into a chain with $k-1$ segment. Denote by Γ_k the ratio of the number of chains with k segments that lose a segment per unit time (due to the annihilation process) to the entire number of these chains N_k. The parameter Γ_k is proportional to the number of thermal fluctuations (per unit time) that induce detachment of side-groups and the number of side-groups per macromolecule. As both these quantities linearly increase with k, one can write

$$\Gamma_k = \Gamma k^2, \tag{7}$$

where Γ is a temperature-dependent material parameter. The kinetic equation for the fragmentation–annihilation process reads

$$\frac{dN_k}{dt}(t) = -\gamma(k-1)N_k(t) + 2\gamma \sum_{j=k+1}^{\infty} N_j(t) + \Gamma\Big[(k+1)^2 N_{k+1}(t) - k^2 N_k(t)\Big].$$

Introducing the concentrations of chains with k segments,

$$n_k(t) = \frac{N_k(t)}{\bar{N}_0}, \tag{8}$$

where $\bar{N}_0 = \bar{N}(0)$ is the total number of chains at the initial instant $t = 0$, we present this equation in the form

$$\frac{dn_k}{dt}(t) = -\gamma(k-1)n_k(t) + 2\gamma \sum_{j=k+1}^{\infty} n_j(t) + \Gamma\Big[(k+1)^2 n_{k+1}(t) - k^2 n_k(t)\Big]. \tag{9}$$

An explicit solution

Our purpose now is to analyze changes in the number-average molecular weight $M_{\rm n}$ and the mass-average molecular weight $M_{\rm w}$ determined by the conventional relations

$$M_{\rm n}(t) = \frac{\sum_{k=1}^{\infty} k n_k(t)}{\sum_{k=1}^{\infty} n_k(t)}, \qquad M_{\rm w}(t)(t) = \frac{\sum_{k=1}^{\infty} k^2 n_k(t)}{\sum_{k=1}^{\infty} k n_k(t)}, \tag{10}$$

when the functions $n_k(t)$ are governed by Eq. (9) with an arbitrary initial condition

$$n_k(0) = n_{0\,k} \qquad (k = 1, 2, \ldots).$$

Following common practice, it is convenient to suppose that the number of segments in a chain is large compared to unity and to replace the discrete index k in Eq. (9) by a continuous argument x. This results in the integro-differential equation for the function $n(t, x)$,

$$\frac{\partial n}{\partial t}(t, x) = -\gamma x n(t, x) + 2\gamma \int_x^{\infty} n(t, y) dy + \Gamma \frac{\partial}{\partial x}\Big(x^2 n(t, x)\Big), \qquad n(0, x) = n_0(x), \tag{11}$$

where $n_0(x)$ is a given function. We do not formulate boundary conditions for the function $n(t, x)$, but assume that this function does not grow very strongly at $x = 0$ and decays rapidly at $x \to \infty$ in the sense that the integrals exist

$$M_m(t) = \int_0^{\infty} x^m n(t, x) dx \qquad (m = 0, 1, 2, \ldots). \tag{12}$$

Multiplying Eq. (11) by x^m $(m = 0, 1, \ldots)$, integrating over x, and using notation (12), we find that

$$\frac{dM_m}{dt}(t) = -\gamma M_{m+1}(t) + 2\gamma \int_0^{\infty} x^m dx \int_x^{\infty} n(t, y) dy + \Gamma \int_0^{\infty} x^m \frac{\partial}{\partial x}\Big(x^2 n(t, x)\Big) dx. \tag{13}$$

The first integral is transformed by changing the order of integration,

$$\int_0^{\infty} x^m dx \int_x^{\infty} n(t, y) dy = \int_0^{\infty} n(t, y) dy \int_0^{y} x^m dx = \frac{1}{m+1} \int_0^{\infty} y^{m+1} n(t, y) dy = \frac{1}{m+1} M_{m+1}(t).$$

The other integral is calculated by integration by parts,

$$\int_0^{\infty} x^m \frac{\partial}{\partial x}\Big(x^2 n(t, x)\Big) dx = -m \int_0^{\infty} x^{m+1} n(t, x) dx = -m M_{m+1}(t).$$

Substitution of these expressions into Eq. (13) results in the differential equation

$$\frac{dM_m}{dt}(t) = -\gamma\Big(\frac{m-1}{m+1} + \kappa m\Big) M_{m+1}(t) \tag{14}$$

with

$$\kappa = \frac{\Gamma}{\gamma}. \tag{15}$$

Assuming the equivalent network of chains to be monodisperse at the initial instant $t = 0$,

$$n_0(x) = \delta(x - L), \tag{16}$$

where L is the initial length of chains, we solve Eq. (14) by Charlesby's method [42]. As Eq. (14) is linear with respect to the unknown function $n(t,x)$, appropriate formulas for the moments $M_m(t)$ corresponding to an arbitrary initial condition $n_0(x)$ are developed by the superposition method.

The mth moment $M_m(t)$ is expanded into the Taylor series in time,

$$M_m(t) = \sum_{k=0}^{\infty} \frac{M_m^{(k)}(0)}{k!} t^k, \tag{17}$$

where $M_m^{(k)}(0)$ stands for the kth derivative at the point $t = 0$. Substitution of Eq. (17) into Eq. (14) implies that

$$M_m^{(k)}(0) = (-\gamma)^k \prod_{j=0}^{k-1} \Big[\frac{m+j-1}{m+j+1} + \kappa(m+j) \Big] M_{m+k}(0).$$

It follows from Eqs. (12) and (16) that

$$M_m(0) = L^m.$$

Substitution of these expressions into Eq. (17) results in

$$M_m(t) = L^m \Big[1 + \sum_{k=1}^{\infty} A_{mk} (-\gamma t L)^k \Big], \tag{18}$$

where

$$A_{mk} = \frac{1}{k!} \prod_{j=0}^{k-1} \Big[\frac{m+j-1}{m+j+1} + \kappa(m+j) \Big].$$

Introducing the new variable $j' = j + 1$ and omitting the prime, we obtain

$$A_{mk} = \prod_{j=1}^{k} \frac{1}{j} \Big[\frac{m+j-2}{m+j} + \kappa(m+j-1) \Big]. \tag{19}$$

Equation (18) implies that for an arbitrary initial condition $n_0(x)$, the moments $M_m(t)$ are given by

$$M_m(t) = \int_0^{\infty} n_0(x) x^m \Big[1 + \sum_{k=1}^{\infty} A_{mk} (-\gamma t x)^k \Big] dx = M_m(0) + \sum_{k=1}^{\infty} A_{mk} M_{m+k}(0) (-\gamma t)^k. \tag{20}$$

Although Eqs. (19) and (20) provide explicit expressions for the moments $M_m(t)$, they are not convenient for the numerical analysis, because the series converges slowly. These formulas are helpful, however, for the evaluation of changes in $M_m(t)$ at small times, $\gamma t \ll 1$. Neglecting terms beyond the first order of smallness in Eq. (20) and using Eqs. (15) and (19), we find that

$$M_0(t) = M_0(0) + M_1(0)\gamma t, \qquad M_1(t) = M_1(0) - M_2(0)\Gamma t,$$
$$M_2(t) = M_2(0) - M_3(0)\Big(\frac{\gamma}{3} + 2\Gamma\Big) t.$$

According to these equations, changes in the moments $M_0(t)$ and $M_1(t)$ are governed by two different processes: an increase in $M_0(t)$ is driven by fragmentation of chains, whereas a decrease in $M_1(t)$ is induced by annihilation of end- and side-groups. Introducing the notation

$$d_{\rm n}(t) = \frac{M_{\rm n}(t)}{M_{\rm n}(0)}, \qquad d_{\rm w}(t) = \frac{M_{\rm w}(t)}{M_{\rm w}(0)} \tag{21}$$

and using Eqs. (10) and (12), we obtain

$$d_{\rm n}(t) = 1 - \Big(M_{\rm n}(0)\gamma + M_{\rm w}(0)\Gamma\Big)t, \qquad d_{\rm w}(t) = 1 - \Big[M_{\rm w}(0)\Gamma + M_{\rm z}(0)\Big(\frac{\gamma}{3} + 2\Gamma\Big)\Big]t, \tag{22}$$

where $M_{\rm z}(t) = M_3(t)/M_2(t)$.

Fitting of observations

As the series in Eq. (18) converges slowly, we analyze the evolution of the mass-average molecular weight $M_{\rm w}$ with elapsed time t numerically. For this purpose, we integrate Eq. (9) with the initial condition

$$n_{0\,k} = \delta_{kK}, \tag{23}$$

where δ_{ij} denotes the Kronecker delta. Equation (23) corresponds to a monodisperse distribution of chains in an equivalent network that contain K segments at the initial instant. We chose this assumption, because the precise initial distribution of chains in a nanocomposite is unknown. Bearing in mind that if the maximal number of segments in a chain equals K at $t = 0$, no chains with higher number of segments can appear at $t > 0$ due to the fragmentation–annihilation process and using Eq. (15), we re-write Eq. (9) as follows:

$$\frac{dn_k}{dt}(t) = -\gamma(k-1)n_k(t) + 2\gamma\sum_{j=k+1}^{K} n_j(t) + \kappa\Big[(k+1)^2 n_{k+1}(t) - k^2 n_k(t)\Big] \qquad (k = 1, 2, \ldots, K). \tag{24}$$

We fix the value $K = 100$ and integrate Eq. (24) with the step $\Delta t = 0.1$. This, relatively large, step is chosen because the fragmentation rate under consideration γ is quite small (of the order of 10^{-8}).

To find the adjustable parameters γ and κ, we fix some intervals $[0, \gamma_{\max}]$ and $[0, \kappa_{\max}]$, where the "best-fit" parameters γ and κ are assumed to be located, and divide these intervals into J subintervals by the points $\gamma^{(i)} = i\Delta\gamma$, and $\kappa^{(j)} = j\Delta\kappa$ $(i, j = 1, \ldots, J-1)$ with $\Delta\gamma = \gamma_{\max}/J$ and $\Delta\kappa = \kappa_{\max}/J$. For any pair $\{\gamma^{(i)}, \kappa^{(j)}\}$, Eq. (24) with initial condition (23) is integrated by the Runge–Kutta method. The best-fit parameters γ and κ are determined from the condition of minimum of the function

$$F = \sum_{t_m}\Big[d_{\rm w}^{\rm exp}(t_m) - d_{\rm w}^{\rm num}(t_m)\Big]^2,$$

where the sum is calculated over all times t_m at which observations are presented in Figure 13, $d_{\rm w}^{\rm exp}$ is the ratio of mass-average molecular weights measured in the tests, and $d_{\rm w}^{\rm num}$ is given by Eqs. (10) and (21). Figure 13 demonstrates fair agreement between the observations on

specimens annealed at various temperatures T_a and the results of numerical simulation with $\gamma = 7.9 \cdot 10^{-8}$ and $\kappa = 436.0$.

To ensure the accuracy of numerical simulation, we use three tests. First, we verify that at $\kappa = 0$, the first moment M_1 remains independent of time [this conclusion follows from Eq. (14) with $\kappa = 0$]. Secondly, we increase K by twice, decrease the rate of fragmentation γ by twice and check that the moments $M_n(t)$ and $M_w(t)$ remain unchanged. The latter implies that the results of numerical analysis are independent of our choice of $K = 100$. Finally, we perform simulation at relatively small times and confirm that the numerical results for the moments $M_m(t)$ $(m = 0, 1, 2)$ coincide with analytical solution (22).

The rate of fragmentation γ found by matching observations on iPP–MMT nanocomposite is of the same order of magnitude as that determined in [20] for degradation of polystyrene at $T_a = 275$ °C. The parameter κ is of the order of 10^2, which implies that the influence of annihilation of side-groups on the degradation process is substantial [20].

To compare our results of numerical analysis with observations reported by other researchers, we recall that Eq. (3) is based on two hypotheses: (i) the rate of fragmentation γ follows the Arrhenius dependence on the annealing temperature T_a,

$$\gamma = \gamma_0 \exp\Big(-\frac{E}{RT_a}\Big), \tag{25}$$

where E is the activation energy and R is the universal gas constant, and (ii) the ratio κ of the rates of annihilation and fragmentation is independent of annealing temperature T_a. It follows from Eq. (25) that the shift factor A

$$A = \frac{\gamma_0}{\gamma_0^{\rm ref}},$$

is given by Eq. (3) with

$$A_0 = \frac{E}{RT^{\rm ref}}, \qquad A_1 = \frac{E}{R}. \tag{26}$$

Calculating the activation energy E from Eq. (26) and Figure 14, we find that $E = 61.8$ kJ/mol. This value is rather close to the activation energies for thermal degradation of isotactic polypropylene $E = 50$ to 120 kJ/mol determined in [3] based on results of thermo-gravimetrical tests at low conversion factors.

Constitutive equations

Our aim now is to fit the experimental data for storage and loss moduli of the hybrid nanocomposite annealed at various temperatures T_a. For this purpose, we derive constitutive equations for the viscoelastic response of a nanocomposite melt at three-dimensional deformations with small strains, simplify these equations for steady shear oscillations, find adjustable parameters in the stress–strain relations by matching the observations depicted in Figures 1, 2, 4, 5, 7, 8, 10 and 11, and analyze the effect of mass-average molecular weight on the material constants. Our analysis is based on the assumption that the characteristic time for thermal degradation (of the order of a few hours) substantially exceeds the characteristic time for relaxation of stresses in a nanocomposite melt (of the order of a few seconds), which implies that scission of macromolecules and annihilation of side-groups may be disregarded in the analysis of mechanical tests.

With reference to the concept of transient networks, a nanocomposite melt is treated as an equivalent network of strands bridged by temporary junctions (entanglements and physical cross-links whose life-time does not exceed the characteristic time of a mechanical test). A strand whose ends are linked to contiguous junctions is treated as an active one. When an end of an active strand separates from a junction, the strand is transformed into the dangling state. When a free end of a dangling strand captures a nearby junction, the strand returns into the active state. Separation of active strands from their junctions and merging of dangling strands with the network occur at random times when the strands are excited by thermal fluctuations. According to the theory of thermally-activated processes [43], the rate of detachment of strands from temporary junctions Φ is governed by the equation

$$\Phi = \Phi_0 \exp\Big(-\frac{\bar{v}}{k_{\rm B}T}\Big), \tag{27}$$

where Φ_0 is the attempt rate (the number of separation events per strand per unit time), $k_{\rm B}$ is Boltzmann's constant, T is the absolute temperature, and $\bar{v} \geq 0$ is the activation energy for separation of an active strand. The coefficient Φ_0 in Eq. (27) is independent of the activation energy $\bar{v}$ and is determined by the current temperature T only. Confining ourselves to isothermal processes at a reference temperature $T^{\rm ref}$ and introducing the dimensionless activation energy $v = \bar{v}/(k_{\rm B}T^{\rm ref})$, we find from Eq. (27) that

$$\Phi(v) = \Phi_0 \exp(-v). \tag{28}$$

To describe the time-dependent response of a nanocomposite melt, we follow the approach proposed in [25, 26] and suppose that different junctions are characterized by different dimensionless activation energies v. The distribution of active strands in a transient network is determined by the number of active strands per unit mass $\bar{N}_{\rm a}$ and the distribution function $p(v)$. The quantity $\bar{N}_{\rm a}p(v)dv$ equals the number of active strands per unit mass linked to junctions with the dimensionless activation energies u belonging to the interval $[v, v + dv]$.

Separation of active strands from temporary junctions and merging of dangling strands with the network are entirely described by the function $\nu(t, \tau, v)$ that equals the number (per unit mass) of active strands at time $t \geq 0$ linked to temporary junctions with activation energy v which have last merged with the network before instant $\tau \in [0, t]$.

The quantity $\nu(t, t, v)$ equals the number of active strands (per unit mass) with the activation energy v at time t,

$$\nu(t, t, v) = \bar{N}_{\rm a}p(v). \tag{29}$$

The function

$$\varphi(\tau, v) = \frac{\partial \nu}{\partial \tau}(t, \tau, v)\Big|_{t=\tau} \tag{30}$$

determines the rate of reformation for dangling chains: the amount $\varphi(\tau, v)d\tau$ equals the number of dangling strands (per unit mass) that merge with temporary junctions with activation energy v within the interval $[\tau, \tau + d\tau]$. The quantity

$$\frac{\partial \nu}{\partial \tau}(t, \tau, v)\, d\tau$$

is the number of these strands that have not separated from their junctions during the interval $[\tau, t]$. The amount

$$-\frac{\partial \nu}{\partial t}(t, 0, v)\, dt$$

is the number of active strands (per unit mass) that detach (for the first time) from the network within the interval $[t, t + dt]$, while the quantity

$$-\frac{\partial^2 \nu}{\partial t \partial \tau}(t, \tau, v)\, dt d\tau$$

equals the number of strands (per unit mass) that have last merged with the network within the interval $[\tau, \tau + d\tau]$ and separate from the network (for the first time after merging) during the interval $[t, t + dt]$.

The rate of detachment Φ is defined as the ratio of the number of active strands that separate from temporary junctions per unit time to the total number of active strands. Applying this definition to active strands that were connected with the network at the initial instant $t = 0$, and to those that merged with the network within the interval $[\tau, \tau + d\tau]$, we arrive at the differential equations

$$\frac{\partial \nu}{\partial t}(t, 0, v) = -\Phi(v)\nu(t, 0, v), \qquad \frac{\partial^2 \nu}{\partial t \partial \tau}(t, \tau, v) = -\Phi(v)\frac{\partial \nu}{\partial \tau}(t, \tau, v). \tag{31}$$

Integration of Eq. (31) with initial conditions (29) (where we set $t = 0$) and (30) implies that

$$\nu(t, 0, v) = \bar{N}_{\rm a} p(v) \exp\Big[-\Phi(v)t\Big], \qquad \frac{\partial \nu}{\partial \tau}(t, \tau, v) = \varphi(\tau, v) \exp\Big[-\Phi(v)(t - \tau)\Big]. \tag{32}$$

To exclude the function $\varphi(t, v)$ from Eq. (32), we use the identity

$$\nu(t, t, v) = \nu(t, 0, v) + \int_0^t \frac{\partial \nu}{\partial \tau}(t, \tau, v) d\tau. \tag{33}$$

Substitution of expressions (29) and (32) into Eq. (33) results in

$$\bar{N}_{\rm a} p(v) = \bar{N}_{\rm a} p(v) \exp\Big[-\Phi(v)t\Big] + \int_0^t \varphi(\tau, v) \exp\Big[-\Phi(v)(t - \tau)\Big] d\tau. \tag{34}$$

The solution of linear integral equation (34) reads $\varphi(t, v) = \bar{N}_{\rm a} p(v)\Phi(v)$. It follows from this equality and Eq. (32) that

$$\frac{\partial \nu}{\partial \tau}(t, \tau, v) = \bar{N}_{\rm a} p(v)\Phi(v) \exp\Big[-\Phi(v)(t - \tau)\Big]. \tag{35}$$

We adopt the conventional assumptions that (i) the excluded-volume effect and other multi-chain effects are screened for individual strands by surrounding macromolecules, (ii) the energy of interaction between strands can be taken into account with the help of the incompressibility condition, and (iii) thermal oscillations of junctions can be disregarded, and the strain tensor for the motion of junctions at the micro-level coincides with the strain tensor for macro-deformation.

At isothermal deformation with small strains, a strand is treated as an isotropic incompressible medium. The strain energy of an active strand w_0 is determined by the conventional formula

$$w_0 = \mu \hat{e}' : \hat{e}',$$

where μ is an average elastic modulus of a strand, $\hat{e}$ is the strain tensor for transition from the reference (stress-free) state of the strand to its deformed state, the prime stands for the deviatoric component of a tensor, and the colon denotes convolution of two tensors.

According to the affinity hypothesis, the strain energy $\bar{w}_0(t,0)$ of an active strand that has not separated from the network during the interval $[0,t]$ reads

$$w(t,0) = \mu \hat{\epsilon}'(t) : \hat{\epsilon}'(t),$$

where $\hat{\epsilon}(t)$ is the strain tensor for transition from the initial (stress-free) state of the network to its deformed state at time t. With reference to [24], we suppose that stress in a dangling strand totally relaxes before this strand captures a new junction. This implies that the stress-free state of an active strand that merges with the network at time $\tau \geq 0$ coincides with the deformed state of the network at that instant. The mechanical energy of an active strand that has last merged with the network at time $\tau \in [0,t]$ is given by

$$w(t,\tau) = \mu \Big[\hat{\epsilon}(t) - \hat{\epsilon}(\tau)\Big]' : \Big[\hat{\epsilon}(t) - \hat{\epsilon}(\tau)\Big]'.$$

Multiplying the strain energy per strand by the number of active strands per unit mass and summing the mechanical energies of active strands linked to temporary junctions with various activation energies, we find the strain energy per unit mass of an equivalent network

$$W(t) = \mu \int_0^\infty \Big\{ \nu(t,0,v) \hat{\epsilon}'(t) : \hat{\epsilon}'(t) + \int_0^t \frac{\partial \nu}{\partial \tau}(t,\tau,v) \Big[\hat{\epsilon}(t) - \hat{\epsilon}(\tau)\Big]' : \Big[\hat{\epsilon}(t) - \hat{\epsilon}(\tau)\Big]' d\tau \Big\} dv. \qquad (36)$$

Differentiating Eq. (36) with respect to time t and using Eqs. (32), (33) and (35), we arrive at the formula

$$\frac{dW}{dt}(t) = \hat{A}(t) : \frac{d\hat{\epsilon}'}{dt}(t) - B(t), \qquad (37)$$

where

$$\hat{A}(t) = 2\mu \bar{N}_{\rm a} \Big\{ \hat{\epsilon}(t) - \int_0^t \hat{\epsilon}(\tau) d\tau \int_0^\infty \Phi(v) \exp\Big[-\Phi(v)(t-\tau)\Big] p(v) dv \Big\}', \qquad (38)$$

$$B(t) = \mu \int_0^\infty \Phi(v) \Big\{ \nu(t,0,v) \hat{\epsilon}'(t) : \hat{\epsilon}'(t) + \int_0^t \frac{\partial \nu}{\partial \tau}(t,\tau,v) \Big[\hat{\epsilon}(t) - \hat{\epsilon}(\tau)\Big]' : \Big[\hat{\epsilon}(t) - \hat{\epsilon}(\tau)\Big]' d\tau \Big\} dv \geq 0. \qquad (39)$$

For isothermal deformation of an incompressible medium, the Clausius–Duhem inequality reads

$$Q = -\frac{dW}{dt} + \frac{\hat{\sigma}'}{\rho} : \frac{d\hat{\epsilon}'}{dt} \geq 0,$$

where ρ is density, Q is internal dissipation per unit mass, and $\hat{\sigma}$ stands for the stress tensor. Substitution of Eq. (37) into this equation implies that

$$Q(t) = \frac{1}{\rho} \Big[\hat{\sigma}'(t) - \rho \hat{A}(t)\Big] : \frac{d\hat{\epsilon}'}{dt}(t) + B(t) \geq 0. \qquad (40)$$

As the function $B(t)$ is non-negative, see Eq. (39), dissipation inequality (40) is satisfied, provided that the expression in the square brackets vanishes. This assertion together with Eq. (38) results in the constitutive equation

$$\hat{\sigma}(t) = -P(t)\hat{I} + 2G\Big\{\hat{\epsilon}'(t) - \int_0^t \hat{\epsilon}'(\tau)d\tau \int_0^\infty \Phi(v)\exp\Big[-\Phi(v)(t-\tau)\Big]p(v)dv\Big\}, \qquad (41)$$

where $P(t)$ is pressure, $\hat{I}$ is the unit tensor, and $G = \rho\mu\bar{N}_{\rm a}$ is an analog of the shear modulus. Formula (41) describes the time-dependent response of an equivalent network at arbitrary three-dimensional deformations with small strains. In what follows, we confine ourselves to shear tests with

$$\hat{\epsilon}(t) = \epsilon(t)\mathbf{e}_1\mathbf{e}_2,$$

where $\epsilon(t)$ is the shear strain, and $\mathbf{e}_m$ $(m = 1, 2, 3)$ are unit vectors of a Cartesian frame. According to Eq. (41), the shear stress $\sigma(t)$ is given by

$$\sigma(t) = 2G\Big\{\epsilon(t) - \int_0^t \epsilon(\tau)d\tau \int_0^\infty \Phi(v)\exp\Big[-\Phi(v)(t-\tau)\Big]p(v)dv\Big\}. \qquad (42)$$

It follows from Eq. (42) that in a shear oscillation test with

$$\epsilon(t) = \epsilon_0\exp(i\omega t),$$

where ϵ_0 and ω are the amplitude and frequency of oscillations, and $i = \sqrt{-1}$, the transient complex modulus

$$\bar{G}^*(t,\omega) = \frac{\sigma(t)}{2\epsilon(t)}$$

is determined by the formula

$$\bar{G}^*(t,\omega) = G\Big\{1 - \int_0^\infty \Phi(v)p(v)dv \int_0^t \exp\Big[-\Big(\Phi(v) + i\omega\Big)s\Big]ds\Big\},$$

where $s = t - \tau$. This equality implies that the steady-state complex modulus

$$G^*(\omega) = \lim_{t\to\infty} \bar{G}^*(t,\omega)$$

is given by

$$G^*(\omega) = G\int_0^\infty \frac{i\omega}{\Phi(v) + i\omega}p(v)dv.$$

This equality together with Eq. (28) implies that the steady-state storage $G'(\omega)$ and loss $G''(\omega)$ shear moduli read

$$\begin{aligned} G'(\omega) &= G\int_0^\infty \frac{\omega^2}{\Phi_0^2\exp(-2v) + \omega^2}p(v)dv, \\ G''(\omega) &= G\int_0^\infty \frac{\Phi_0\exp(-v)\omega}{\Phi_0^2\exp(-2v) + \omega^2}p(v)dv. \end{aligned} \qquad (43)$$

To fit the experimental data, we adopt the random energy model [44] with the quasi-Gaussian distribution function $p(v)$,

$$p(v) = p_0\exp\Big[-\frac{(v-V)^2}{2\Sigma^2}\Big] \quad (v \geq 0), \qquad p(v) = 0 \quad (v < 0), \qquad (44)$$

where V and Σ are adjustable parameters (the apparent average activation energy and the apparent standard deviation of activation energies, respectively), and the constant p_0 is found from the normalization condition

$$\int_0^\infty p(v)dv = 1. \tag{45}$$

Governing equations (43) and (44) involve four material constants: (i) the instantaneous shear modulus G, (ii) the attempt rate for rearrangement of strands Φ_0, (iii) an analog of the average activation energy for rearrangement of strands in a network V, and (iv) an analog of the standard deviation of activation energies Σ.

When the dimensionless ratio $\xi = \Sigma/V$ is small compared to unity (it will be shown later that this condition is satisfied for our experimental data), the number of adjustable parameters may be reduced to three. Assuming that

$$\frac{\Sigma}{V} \ll 1, \tag{46}$$

we can employ the first equality in Eq. (44) for an arbitrary (positive and negative) v. Replacing the lower limit of integration in Eqs. (43) by $-\infty$, we obtain

$$\begin{aligned} G'(\omega) &= Gp_0 \int_{-\infty}^{\infty} \frac{\omega^2}{\Phi_0^2 \exp(-2v) + \omega^2} \exp\Big[-\frac{(v-V)^2}{2\Sigma^2}\Big] dv, \\ G''(\omega) &= Gp_0 \int_{-\infty}^{\infty} \frac{\Phi_0 \exp(-v)\omega}{\Phi_0^2 \exp(-2v) + \omega^2} \exp\Big[-\frac{(v-V)^2}{2\Sigma^2}\Big] dv, \end{aligned} \tag{47}$$

where

$$p_0 = \frac{1}{2\pi\sqrt{\Sigma}}.$$

To exclude the attempt rate Φ_0 from the consideration, we introduce the notation

$$\Phi_0 = \Phi_* \exp(v_0),$$

where Φ_* is a given value (in what follows, we set $\Phi_* = 10^{10}$ s^{-1}), and $v_0 = \ln \Phi_0/\Phi_*$. Substituting this expression into Eq. (47) and introducing the new variable $v' = v - v_0$, we find that

$$\begin{aligned} G'(\omega) &= Gp_0 \int_{-\infty}^{\infty} \frac{\omega^2}{\Phi_*^2 \exp(-2v') + \omega^2} \exp\Big[-\frac{(v'-V')^2}{2\Sigma^2}\Big] dv', \\ G''(\omega) &= Gp_0 \int_{-\infty}^{\infty} \frac{\Phi_* \exp(-v')\omega}{\Phi_*^2 \exp(-2v') + \omega^2} \exp\Big[-\frac{(v'-V')^2}{2\Sigma^2}\Big] dv', \end{aligned}$$

where

$$V' = V - v_0 = V - \ln\frac{\Phi_0}{\Phi_*}.$$

Omitting primes for the sake of simplicity and replacing the lower limits of integration by zero, we return to Eqs. (43), where the unknown attempt rate Φ_0 is replaced by Φ_*. This implies that each set of observations for the storage and loss shear moduli, $G'(\omega)$ and $G''(\omega)$, is entirely determined by three quantities: G, V and Σ. For hybrid nanocomposites subjected to thermal treatment, these parameters are functions of annealing temperature T_a and annealing time t_a.

Fitting of observations

To assess the effect of temperature and time of annealing, we determine the quantities G, V and Σ by matching the experimental data depicted in Figures 1, 2, 4, 5, 7, 8, 10 and 11. Each set of observations for $G'(\omega)$ and $G''(\omega)$ is approximated separately. We fix some intervals $[0, V_{\max}]$ and $[0, \Sigma_{\max}]$, where the "best-fit" parameters V and Σ are assumed to be located, and divide these intervals into J subintervals by the points $V^{(i)} = i\Delta V$ and $\Sigma^{(j)} = j\Delta\Sigma$ $(i, j = 1, \ldots, J-1)$ with $\Delta V = V_{\max}/J$ and $\Delta\Sigma = \Sigma_{\max}/J$. For any pair $\{V^{(i)}, \Sigma^{(j)}\}$, the coefficient p_0 in Eq. (44) is calculated from Eq. (45), where the integral is evaluated numerically by Simpson's method with 400 points and the step $\Delta v = 0.1$. The integrals in Eq. (43) are calculated by using the same technique. The shear modulus G is found by the least-squares method from the condition of minimum of the function

$$F = \sum_{\omega_m} \Big\{ \Big[G'_{\exp}(\omega_m) - G'_{\mathrm{num}}(\omega_m) \Big]^2 + \Big[G''_{\exp}(\omega_m) - G''_{\mathrm{num}}(\omega_m) \Big]^2 \Big\},$$

where the sum is calculated over all experimental points ω_m, $G'_{\exp}$ and $G''_{\exp}$ are the storage and loss moduli measured in a test, and G'_{num} and G''_{num} are given by Eq. (43). The "best-fit" parameters V and Σ are determined from the condition of minimum of the function F on the set $\{V^{(i)}, \Sigma^{(j)} \quad (i, j = 1, \ldots, J-1)\}$. After finding the "best-fit" values $V^{(i)}$ and $\Sigma^{(j)}$, this procedure is repeated twice for the new intervals $[V^{(i-1)}, V^{(i+1)}]$ and $[\Sigma^{(j-1)}, \Sigma^{(j+1)}]$, to ensure an acceptable accuracy of fitting. Figures 1, 2, 4, 5, 7, 8, 10 and 11 demonstrate excellent agreement between the experimental data and the results of numerical simulation.

For each annealing time t_{a} and annealing temperature T_{a}, we (i) find the ratio of mass-average molecular weights d_{w} from Eqs. (1) and (2) and the observations depicted in Figures 3, 6, 9 and 12, (ii) calculate the material constants G, V and Σ by matching the experimental data reported in Figures 1, 2, 4, 5, 7, 8, 10 and 11, and (iii) plot the quantities G, V and Σ versus d_{w} in Figures 17 and 18. The experimental data are approximated by the linear equations

$$G = G_0 + G_1 d_{\mathrm{w}}, \qquad V = V_0, \qquad \Sigma = \Sigma_0 + \Sigma_1 d_{\mathrm{w}}, \tag{48}$$

where the coefficients G_i, V_i and Σ_i $(i = 0, 1)$ are calculated by the least-squares method. Figures 17 and 18 show that Eq. (48) correctly describes changes in the adjustable parameters with mass-average molecular weight. The average activation energy for separation of strands from temporary junctions V is independent of molecular weight, whereas the shear modulus G and the standard deviation of activation energies Σ noticeably grow with M_{w}. It can also be seen from Figure 18 that inequality (46) is satisfied with a reasonable level of accuracy (the ratio on left-hand side of Eq. (46) does not exceed 0.2).

Discussion

We begin with the analysis of material constants in Eq. (1) that describes the effect of frequency of oscillations ω on the modulus of complex viscosity η. According to Figure 15, the exponent α is practically independent of mass-average molecular weight. It follows from this conclusion and Eq. (1) that the curves $\eta(\omega)$ measured at various annealing temperatures T_{a} and annealing times t_{a} and plotted in double-logarithmic coordinates may be superposed (with a high level of accuracy) by shifts along the horizontal (frequency) and vertical (viscosity) axes.

Figure 16 demonstrates that the characteristic time τ linearly decreases with mass-average molecular weight. This implies that the reciprocal quantity τ^{-1} (with the dimension of rate) linearly grows with $M_{\rm w}$. The latter conclusion is in agreement with observations by Bywater and Black [45], who found a similar trend for the degradation rate of poly(methyl methacrylate) and poly(α-methylstyrene).

Figure 17 shows that the elastic modulus G linearly increases with mass-average molecular weight. A linear relation between the shear modulus and the molecular weight between entanglements $M_{\rm e}$ provides a basis for the statistical theory of rubber elasticity. It follows from this dependence and Figure 17 that the molecular weight between entanglements $M_{\rm e}$ is proportional to the mass-average molecular weight $M_{\rm w}$. The latter result appears to be quite natural.

According to Figure 18, the average energy for detachment of strands from temporary junctions V is independent of molecular weight. This result seems natural as well. Indeed, for a melt of a hybrid nanocomposite, the average activation energy V may be treated as the energy of thermal fluctuations necessary for mutual displacement of two chains (or for detachment of a chain from a stack of clay platelets) to a distance at which the two chains (or the chain and the filler particle) weakly affect each other. It seems plausible to assume that this parameter is independent of the chains' length (because it reflects local interactions between their segments). The latter implies that thermal degradation of a nanocomposite melt (modelled as scission of chains and annihilation of end- and side groups) should not affect V, which is confirmed by the experimental data presented in Figure 18.

Figure 18 reveals that the standard deviation of activation energies Σ linearly increases with mass-average molecular weight. To provide an explanation for this observation, we recall that the standard deviation of activation energies Σ may be thought of as a measure of heterogeneity of an equivalent network of macromolecules, see Eq. (44). Thermal degradation of a polymer matrix results in homogenization of the network (as the rates of scission of macromolecules and detachment of side-groups are proportional to chains' lengths), which is observed as a reduction in Σ with a decrease in $d_{\rm w}$. It is worth noting that a similar decrease in the inhomogeneity of an equivalent network driven by thermal degradation of neat iPP was previously observed as a reduction in the polydispersity index with annealing time [3].

Figures 15 to 18 show that the adjustable parameters in the model are not affected by the history of thermal pre-treatment, but are determined by the current mass-average molecular weight $M_{\rm w}$ exclusively. Some scatter should, however, be mentioned of the experimental data depicted in these figures. It may be explained by the fact that at each temperature $T_{\rm a}$ and each annealing time $t_{\rm a}$, a new sample was used for testing, whose physical properties do not exactly coincide with those of other specimens.

Concluding remarks

A series of torsional oscillation tests with small strains have been performed at the temperature $T = 230$ °C on a hybrid nanocomposite with a polypropylene matrix reinforced with 5 wt.% of MMT clay. Prior to mechanical tests, specimens were annealed at the temperatures $T_{\rm a} = 250$, 270, 290 and 310 °C for various amounts of time $t_{\rm a}$ ranging from 15 to 420 min. Thermal treatment induced thermal degradation of samples observed as a pronounced decrease in their mass-average molecular weight with exposure time $t_{\rm a}$.

With reference to the fragmentation–annihilation concept, a kinetic equation has been developed for the concentration of chains with various lengths. This relation involves two adjustable parameters that are found by matching the experimental data for the evolution of mass-average molecular weight. In addition to the numerical analysis, an explicit solution of the kinetic equation has been derived.

A constitutive model has been developed for the viscoelastic response of a nanocomposite melt at isothermal three-dimensional deformations with small strains. The melt is treated as an equivalent transient network of strands bridged by temporary junctions. Its time-dependent behavior is modelled as separation of active strands from their junctions and attachment of dangling strands to the network. The rearrangement events occur at random times, when appropriate strands are thermally activated.

Stress–strain relations for an equivalent heterogeneous network of strands (where different junctions have different activation energies for rearrangement of strands) have been derived by using the laws of thermodynamics. The constitutive equations involve three material parameters that are determined by matching the experimental data for the storage and loss moduli as functions of frequency of oscillations ω. Fair agreement is demonstrated between the observations and the results of numerical simulation.

The following conclusions are drawn:

1. The average activation energy for rearrangement of strands in a transient network V is practically independent of molecular weight.

2. The standard deviation of activation energies Σ and the shear modulus G linearly grow with mass-average molecular weight M_{w}.

3. The values of these parameters are independent of the history of thermal pre-treatment and are entirely determined by the current mass-average molecular weights. This implies that thermal degradation may be used as a quick-and-dirty test directed to establish correlations between the viscoelastic properties and molecular weights of polymers and hybrid nanocomposites.

Acknowledgement

This work was partially supported by the West Virginia Research Challenge Grant Program. The authors are deeply indebted to A. Manivannan for performing WAXD tests.

References

[1] Incarnato, L.; Scarfato, P.; Acierno, D.; Milana, M.R.; Feliciani, R.: J Appl Polym Sci 2003, 89, 1768–1778.

[2] Grassie, N.; Scott, G.: Polymer Degradation and Stabilisation. Cambridge Univ. Press, Cambridge 1985.

[3] Chan, J.H.; Balke, S.T.: Polym Degrad Stab 1997, 57, 113–125, 127–134, 135–149.

[4] Peterson, J.D.; Vyazovkin, S.; Wight, C.A.: Macromol Chem Phys 2001, 202, 775–784.

[5] Fayolle, B.; Audouin, L.; Verdu, J.: Polym Degrad Stab 2002, 75, 123–129.

[6] Gao, Z.; Kaneko, T.; Amasaki, I.; Nakada, M.: Polym Degrad Stab 2003, 80, 269–274.

[7] Manias, E.; Touny, A.; Wu, L.; Strawhecker, K.; Lu, B.; Chung, T.C.: Chem Mater 2001, 13, 3516–3523.

[8] Kodgire, P.; Kalgaonkar, R.; Hambir, S.; Bulakh, N.; Jog, J.P.: J Appl Polym Sci 2001, 81, 1786-1792.

[9] Ma, J.; Qi, Z.; Hu, Y.: J Appl Polym Sci 2001, 82, 3611–3617.

[10] Galgali, G.; Ramesh, C.; Lele, A.: Macromolecules 2001, 34, 852–858.

[11] Koo, C.M.; Kim, M.J.; Choi, M.H.; Kim, S.O.; Chung, I.J.: J Appl Polym Sci 2003, 88, 1526–1535.

[12] Li, J.; Zhou, C.; Wang, G.; Zhao, D.: J Appl Polym Sci 2003, 89, 318–323.

[13] He, J.-D.; Cheung, M.K.; Yang, M.-S.; Qi, Z.: J Appl Polym Sci 2003, 89, 3404-3415.

[14] Kawasumi, M.; Hasegawa, N.; Kato, M.; Usuki, A.; Okada, A.: Macromolecules 1997, 30, 6333–6338.

[15] Solomon, M.J.; Almussallam, A.S.; Seefeldt, K.F.; Somwangthanaroj, A.; Varadam, P.: Macromolecules 2001, 34, 1864–1872.

[16] Svoboda, P.; Zeng, C.; Wang, H.; Lee, L.J.; Tomasko, D.L.: J Appl Polym Sci 2002, 85, 1562–1570.

[17] Ellis, T.S.; D'Angelo, J.S.: J Appl Polym Sci 2003, 90, 1639–1647.

[18] Edwards, B.F.; Cai, M.; Han, H.: Phys Rev A 1990, 41, 5755–5757.

[19] Huang, J.; Edwards, B.F.; Levine, A.D.: J Phys A: Math Gen 1991, 24, 3967–3977.

[20] Drozdov, A.D.: cond-mat/0309677.

[21] Green, M.S.; Tobolsky, A.V.: J Chem Phys 1946, 14, 80–92.

[22] Yamamoto, M.: J Phys Soc Japan 1956, 11, 413–421.

[23] Lodge, A.S.: Rheol Acta 1968, 7, 379–392.

[24] Tanaka, F.; Edwards, S.F.: Macromolecules 1992, 25, 1516–1523.

[25] Drozdov, A.D.; Christiansen, J. deC.: Int J Solids Struct 2003, 40, 1337–1367.

[26] Drozdov, A.D.; Christiansen, J. deC.: Polym Eng Sci 2003, 43, 946–959.

[27] Bensason, S.; Stepanov, E.V.; Chum, S.; Hiltner, A.; Baer, E.: Macromolecules 1997, 30, 2436–2444.

[28] Sweeney, J.; Collins, T.L.D.; Coates, P.D.; Duckett, R.A.: J Appl Polym Sci 1999, 72, 563–575.

[29] Barakos, G.; Mitsoulis, E.; Tzoganakis, C.; Kajiwara, T.: J Appl Polym Sci 1996, 59, 543–556.

[30] Carrot, C.; Revenu, P.; Guillet, J.: J Appl Polym Sci 1996, 61, 1887–1897.

[31] Sugimoto, M.; Masubuchi, Y.; Takimoto, J.; Koyama, K.: J Polym Sci Part B: Polym Phys 2001, 39, 2692–2704.

[32] Sugimoto, M.; Tanaka, T.; Masubuchi, Y.; Takimoto, J.-I.; Koyama, K.: J Appl Polym Sci 2001, 73, 1493–1500.

[33] Fujiyama, M.; Kitajima, Y.; Inata, H.: J Appl Polym Sci 2002, 84, 2128–2141.

[34] Fujiyama, M.; Inata, H.: J Appl Polym Sci 2002, 84, 2157–2170.

[35] Pramoda, K.P.; Liu, T.; Liu, Z.; He, C.; Sue, H.-J.: Polym Degrad Stab 2003, 81, 37–56.

[36] Zhang, Q.; Wang, Y.; Fu, Q.: J Polym Sci Part B: Polym Phys 2003, 41, 1–10.

[37] Yang, W.; Li, Z.-M.; Xie, B.-H.; Feng, J.-M.; Shi, W.; Yang, M.-B.: J Appl Polym Sci 89, 2003, 686–690.

[38] Horrocks, A.R.; Valinejad, K.; Crighton, J.S.: J Appl Polym Sci 1994, 54, 593–600.

[39] Ferry, J.D.: Viscoelastic Properties of Polymers. Wiley, New York 1980.

[40] Nakajima, N.; Wong, P.S.L.: J Appl Polym Sci 1965, 9, 3141–3152.

[41] Gupta, R.K.: In Advani, S.G. (Ed.): Flow and Rheology in Polymer Composites Manifacturing. Elsevier, Amsterdam 1994, pp. 9–51.

[42] Charlesby, A.: Proc Roy Soc London A 1954, 224, 120.

[43] Eyring, H.: J Chem Phys 1936, 4, 283–291.

[44] Derrida, B. Phys Rev Lett 1980, 45, 79–92.

[45] Bywater, S.; Black, P.E.: J Phys Chem 1965, 69, 2967–2970.

List of figures

Figure 1: The storage modulus G' versus frequency ω. Circles: experimental data on iPP–MMT nanocomposite annealed at $T_a = 250$ °C for $t_a = 0$, 60 and 90 min, from top to bottom, respectively. Solid lines: results on numerical simulation

Figure 2: The loss modulus G'' versus frequency ω. Circles: experimental data on iPP–MMT nanocomposite annealed at $T_a = 250$ °C for $t_a = 0$, 60 and 90 min, from top to bottom, respectively. Solid lines: results on numerical simulation

Figure 3: The complex viscosity η versus frequency ω. Circles: experimental data on iPP–MMT nanocomposite annealed at $T_a = 250$ °C for $t_a = 0$, 60 and 90 min, from top to bottom, respectively. Solid lines: results on numerical simulation

Figure 4: The storage modulus G' versus frequency ω. Circles: experimental data on iPP–MMT nanocomposite annealed at $T_a = 270$ °C for $t_a = 0$, 60 and 90 min. Solid lines: results on numerical simulation

Figure 5: The loss modulus G'' versus frequency ω. Circles: experimental data on iPP–MMT nanocomposite annealed at $T_a = 270$ °C for $t_a = 0$, 60 and 90 min. Solid lines: results on numerical simulation

Figure 6: The complex viscosity η versus frequency ω. Circles: experimental data on iPP–MMT annealed at $T_a = 270$ °C for $t_a = 0$, 60 and 90 min, from top to bottom, respectively. Solid lines: results on numerical simulation

Figure 7: The storage modulus G' versus frequency ω. Circles: experimental data on iPP–MMT nanocomposite annealed at $T_a = 290$ °C for $t_a = 0$, 15, 30, 60, 120 and 420 min, from top to bottom, respectively. Solid lines: results on numerical simulation

Figure 8: The loss modulus G'' versus frequency ω. Circles: experimental data on iPP–MMT nanocomposite annealed at $T_a = 290$ °C for $t_a = 0$, 15, 30, 60, 120 and 420 min, from top to bottom, respectively Solid lines: results on numerical simulation

Figure 9: The complex viscosity η versus frequency ω. Circles: experimental data on iPP–MMT nanocomposite annealed at $T_a = 290$ °C for $t_a = 0$, 15, 30, 60, 120 and 420 min, from top to bottom, respectively. Solid lines: results on numerical simulation

Figure 10: The storage modulus G' versus frequency ω. Circles: experimental data on iPP–MMT nanocomposite annealed at $T_a = 310$ °C for $t_a = 0$, 15, 30 and 60 min, from top to bottom, respectively. Solid lines: results on numerical simulation

Figure 11: The loss modulus G'' versus frequency ω. Circles: experimental data on iPP–MMT nanocomposite annealed at $T_a = 310$ °C for $t_a = 0$, 15, 30 and 60 min, from top to bottom, respectively. Solid lines: results on numerical simulation

Figure 12: The complex viscosity η versus frequency ω. Circles: experimental data on iPP–MMT nanocomposite annealed at $T_a = 310$ °C for $t_a = 0$, 15, 30 and 60 min, from top to bottom, respectively. Solid lines: results on numerical simulation

Figure 13: The ratio of mass-average molecular weights d_w versus annealing time t_a. Symbols: experimental data on iPP–MMT nanocomposite annealed at temperatures T_a °C. Unfilled circles: $T_a = 250$; filled circles: $T_a = 270$; asterisks: $T_a = 290$; stars: $T_a = 310$. Solid line: results of numerical simulation

Figure 14: The shift factor A versus annealing temperature T_a. Circles: experimental data on iPP–MMT nanocomposite. Solid line: approximation of the experimental data by Eq. (3) with $A_0 = 13.32$ and $A_1 = 7.43 \cdot 10^3$

Figure 15: The dimensionless exponent α versus the ratio of mass-average molecular weights d_w. Symbols: treatment of observations on iPP–MMT nanocomposite at annealing temperatures T_a °C. Unfilled circles: $T_a = 250$; filled circles: $T_a = 270$; asterisks: $T_a = 290$; stars: $T_a = 310$. Solid line: approximation of the experimental data by Eq. (4) with $\alpha_0 = 0.68$ and $\alpha_1 = 0.17$

Figure 16: The characteristic time τ versus the ratio of mass-average molecular weights d_w. Symbols: treatment of observations on iPP–MMT nanocomposite at annealing temperatures T_a °C. Unfilled circles: $T_a = 250$; filled circles: $T_a = 270$; asterisks: $T_a = 290$; stars: $T_a = 310$. Solid line: approximation of the experimental data by Eq. (4) with $\tau_0 = -0.39$ and $\tau_1 = 0.95$

Figure 17: The instantaneous shear modulus G versus the ratio of mass-average molecular weights d_w. Symbols: treatment of observations on iPP–MMT nanocomposite at annealing temperatures T_a °C. Unfilled circles: $T_a = 250$; filled circles: $T_a = 270$; asterisks: $T_a = 290$; stars: $T_a = 310$. Solid line: approximation of the experimental data by Eq. (48) with $G_0 = -0.07$ and $G_1 = 0.32$

Figure 18: The average activation energy for rearrangement of strands V and the standard deviation of activation energies Σ versus the ratio of mass-average molecular weights d_w. Symbols: treatment of observations on iPP–MMT nanocomposite at annealing temperatures T_a °C. Unfilled circles: $T_a = 250$; filled circles: $T_a = 270$; asterisks: $T_a = 290$; stars: $T_a = 310$. Solid lines: approximation of the experimental data by Eq. (48) with $V_0 = 15.82$ (curve 1) and $\Sigma_0 = 0.95$ and $\Sigma_1 = 1.93$ (curve 2)

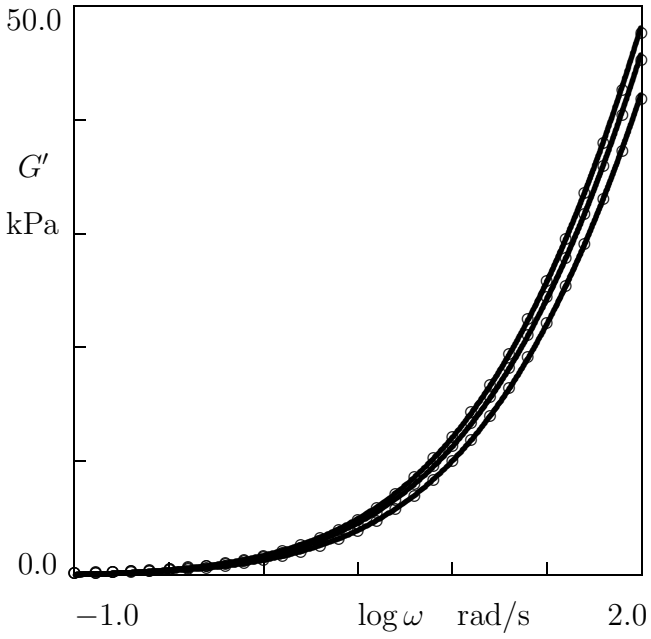

Figure 1:

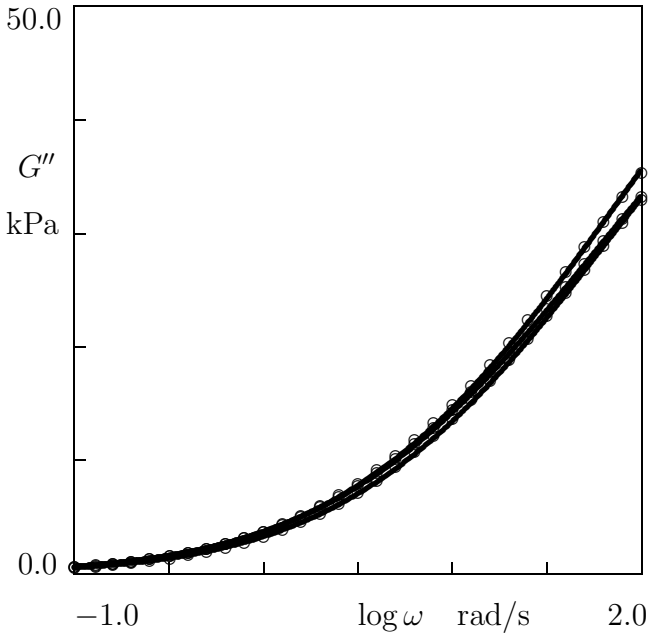

Figure 2:

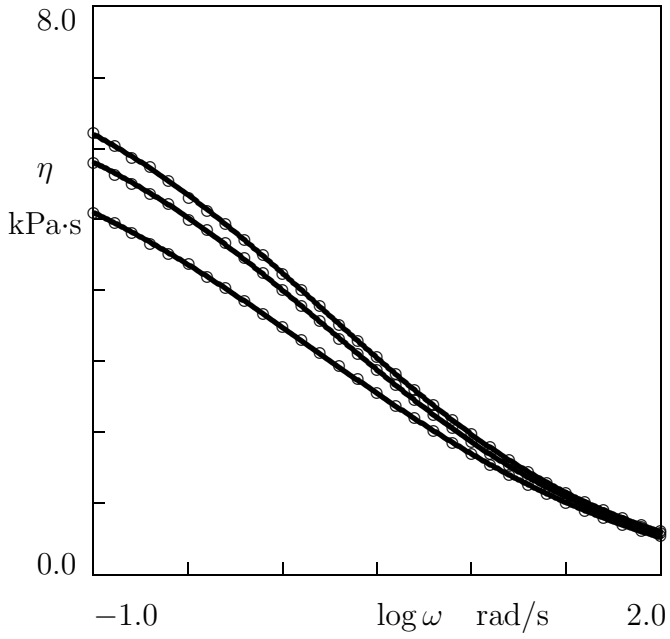

Figure 3:

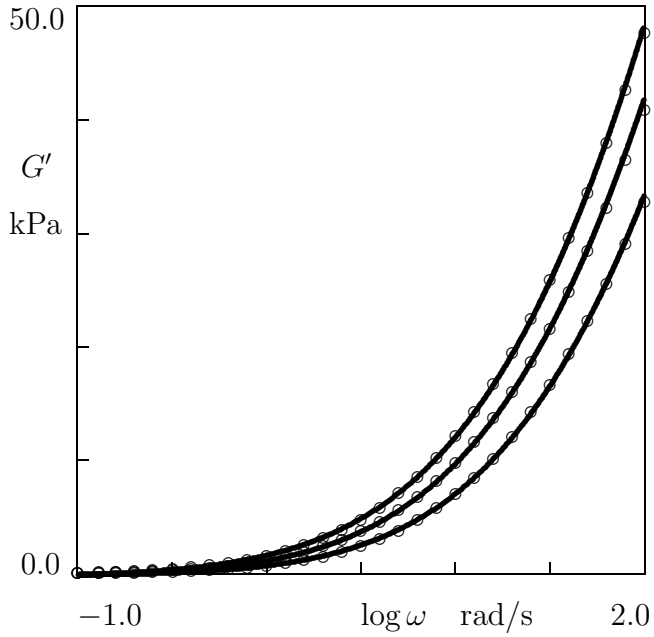

Figure 4:

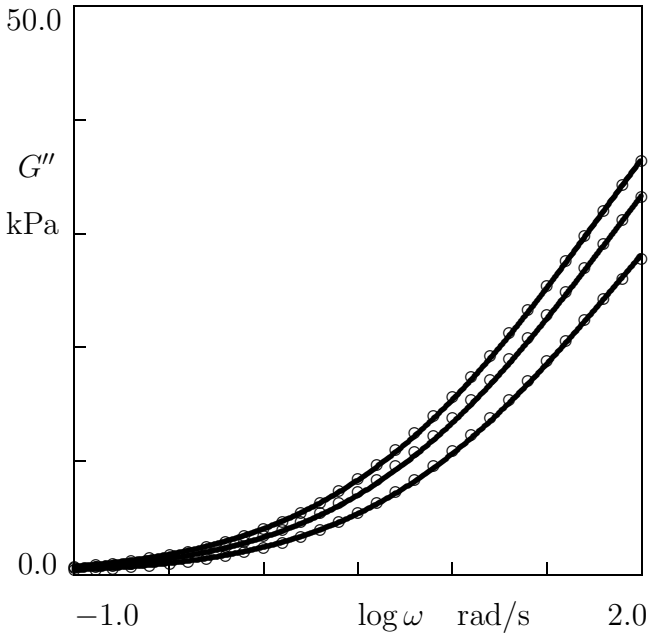

Figure 5:

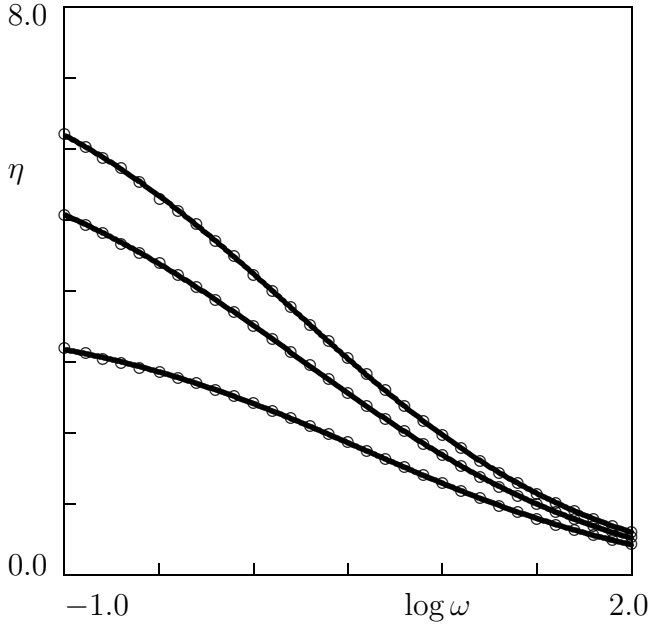

Figure 6:

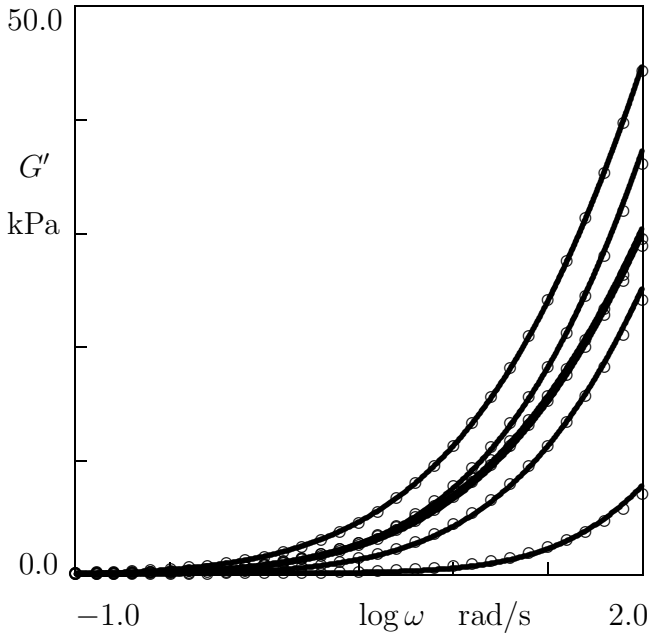

Figure 7:

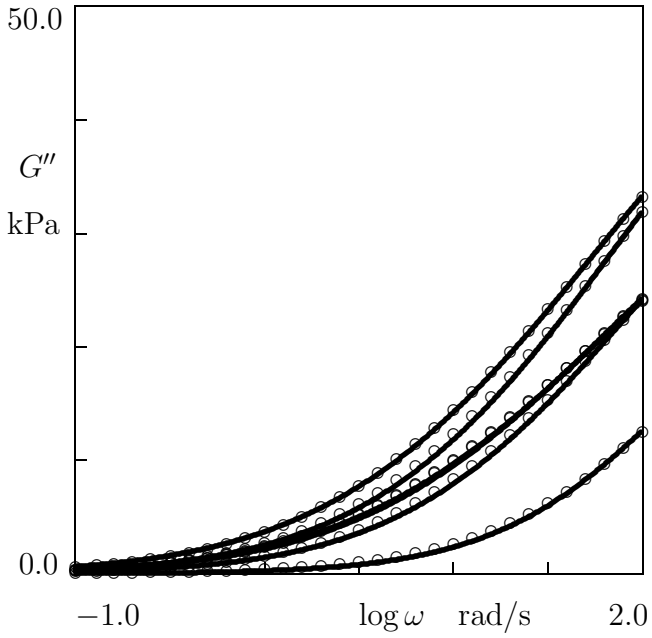

Figure 8:

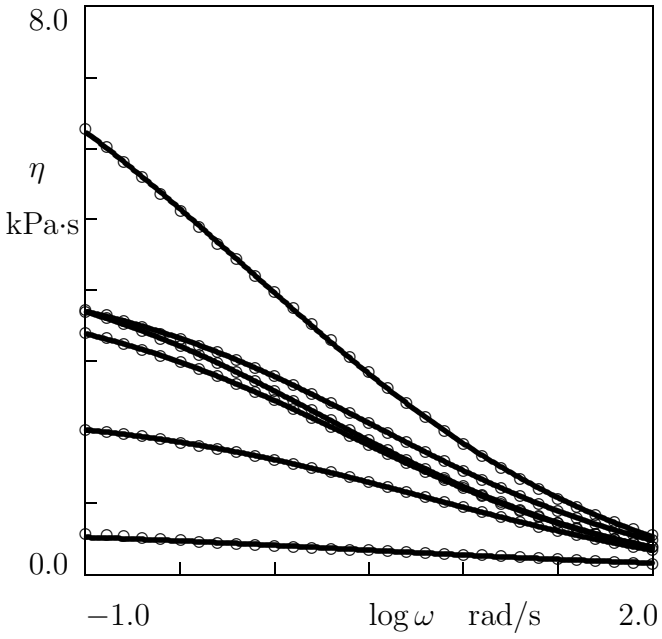

Figure 9:

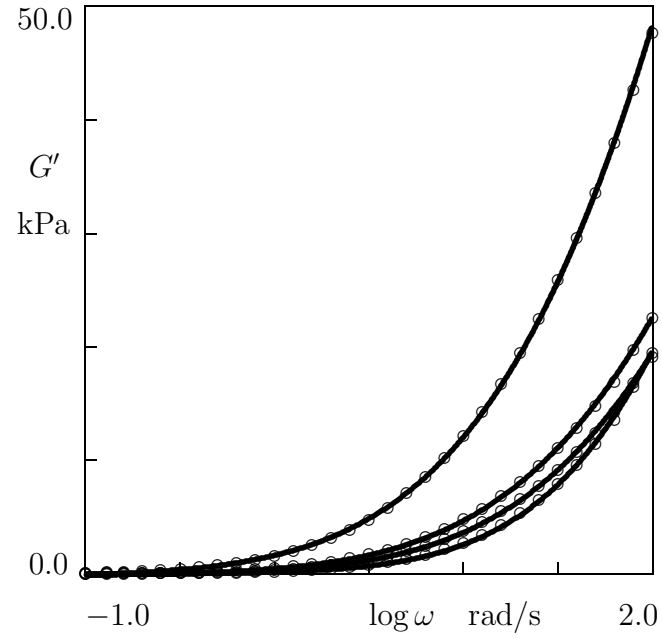

Figure 10:

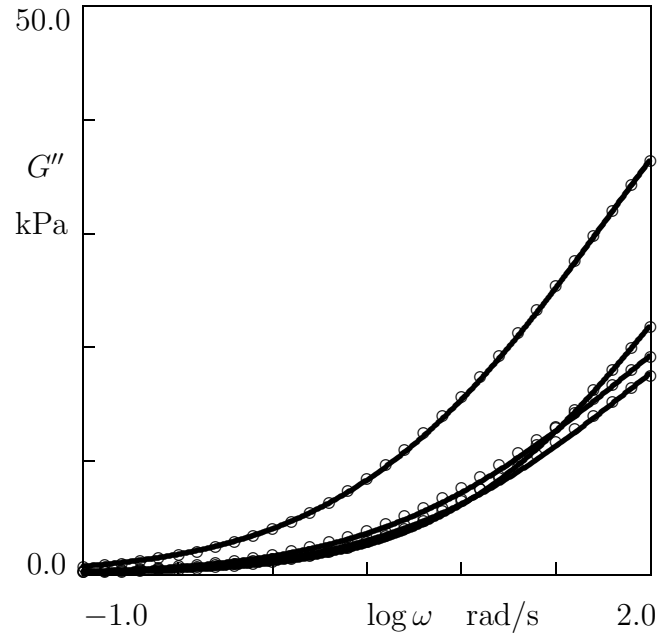

Figure 11:

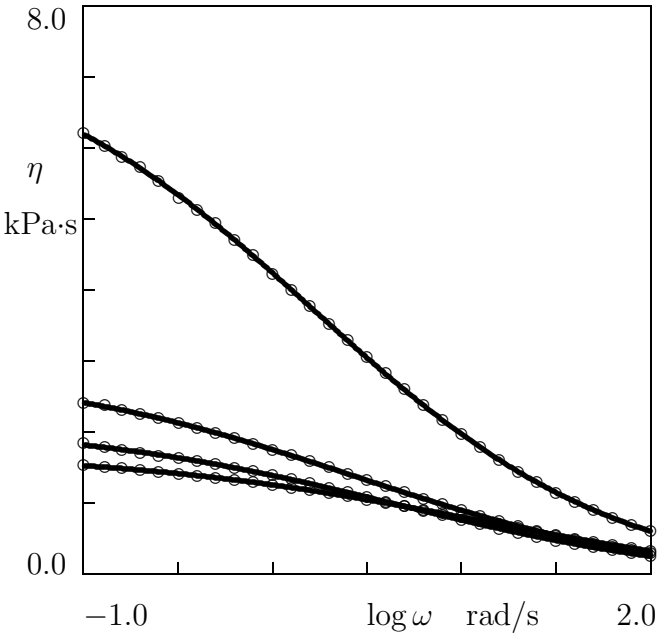

Figure 12:

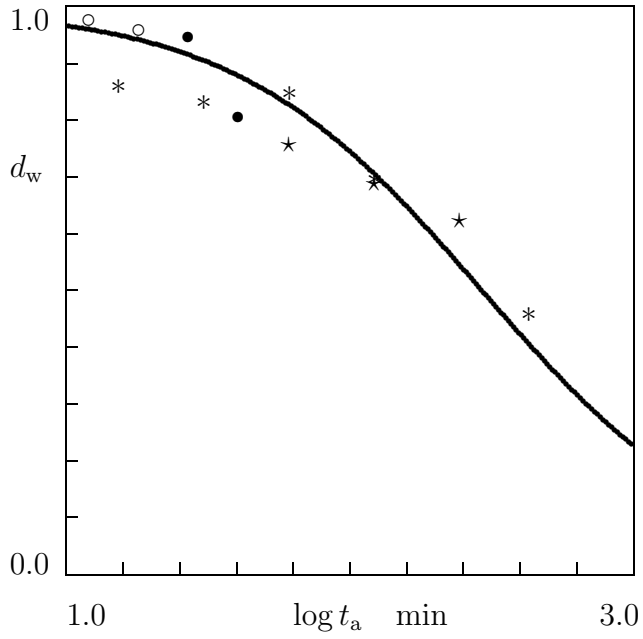

Figure 13:

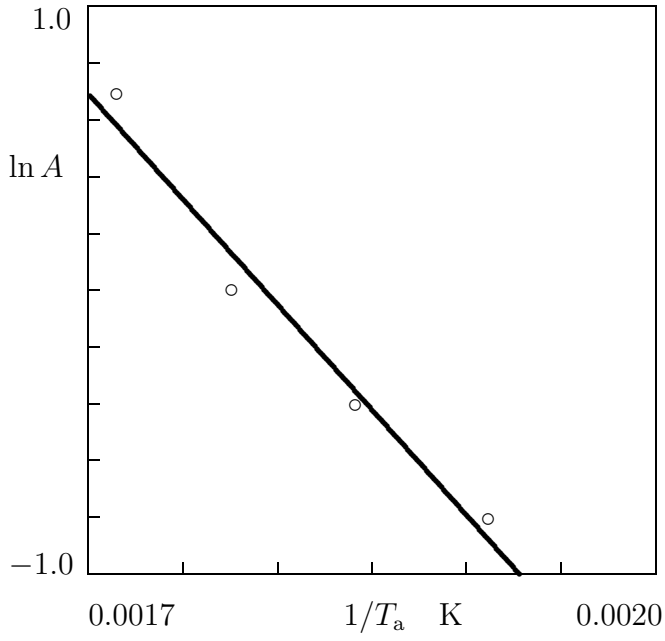

Figure 14:

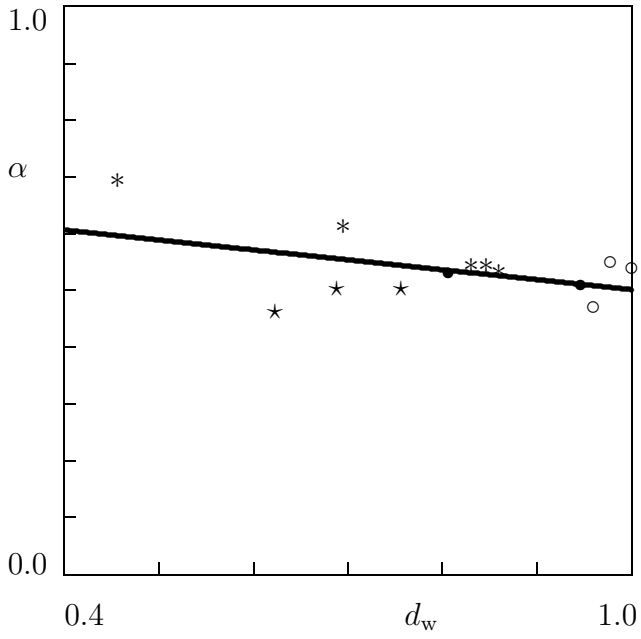

Figure 15:

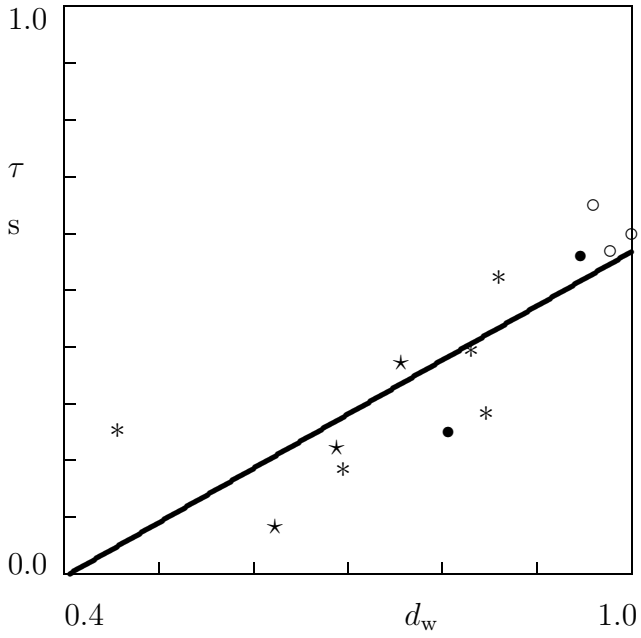

Figure 16:

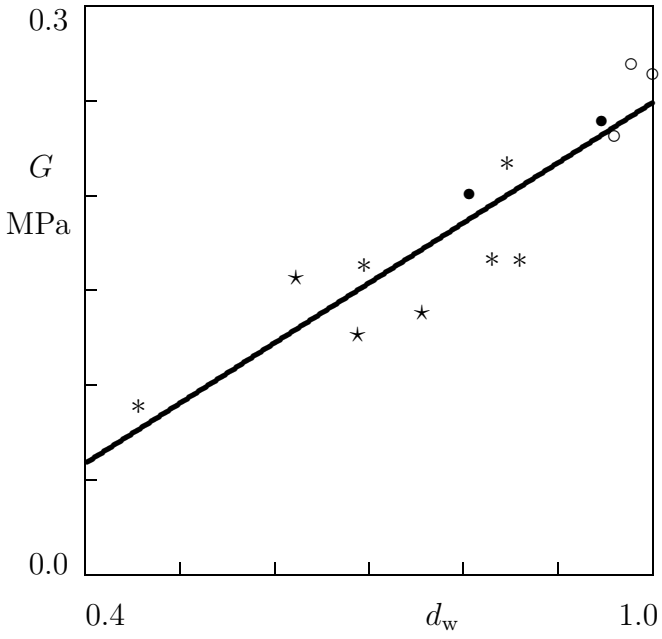

Figure 17:

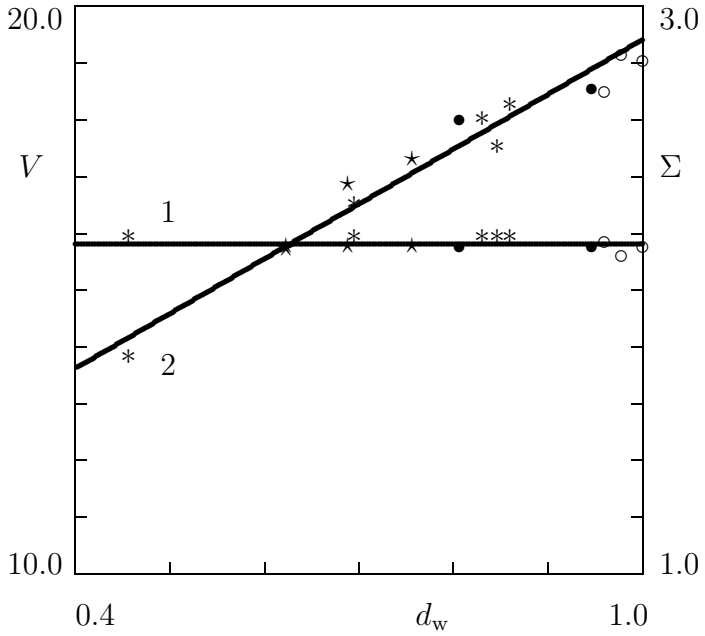

Figure 18: